

Development of Eco-Friendly Ag Embedded Peroxo Titanium Complex Solution Based Thin Film and Electrical Behaviors of Resistive Random Access Memory

Won Jin Kim^{1*}, Jinho Lee^{2*}, Ryun Na Kim², Donghee Lee², and Woo-Byoung Kim^{1,2†}

¹Department of Foundry Engineering, Dankook University, Younjin 16890, Republic of Korea

²Department of Energy Engineering, Dankook University, Cheonan 31116, Republic of Korea

(Received February 16, 2024 : Revised March 20, 2024 : Accepted March 21, 2024)

Abstract In this study, we introduce a novel TiN/Ag embedded TiO₂/FTO resistive random-access memory (RRAM) device. This distinctive device was fabricated using an environmentally sustainable, solution-based thin film manufacturing process. Utilizing the peroxo titanium complex (PTC) method, we successfully incorporated Ag precursors into the device architecture, markedly enhancing its performance. This innovative approach effectively mitigates the random filament formation typically observed in RRAM devices, and leverages the seed effect to guide filament growth. As a result, the device demonstrates switching behavior at substantially reduced voltage and current levels, heralding a new era of low-power RRAM operation. The changes occurring within the insulator depending on Ag contents were confirmed by X-ray photoelectron spectroscopy (XPS) analysis. Additionally, we confirmed the correlation between Ag and oxygen vacancies (V_o). The current-voltage (*I-V*) curves obtained suggest that as the Ag content increases there is a change in the operating mechanism, from the space charge limited conduction (SCLC) model to ionic conduction mechanism. We propose a new filament model based on changes in filament configuration and the change in conduction mechanisms. Further, we propose a novel filament model that encapsulates this shift in conduction behavior. This model illustrates how introducing Ag alters the filament configuration within the device, leading to a more efficient and controlled resistive switching process.

Key words resistive random-access memory, peroxo titanium complex, resistive switching, Ag embedded TiO₂, conduction mechanism.

1. Introduction

The advancement of technologies such as big data and artificial intelligence (A.I) necessitates faster digital information processing compared to previous times.¹⁾ However, scaling down existing silicon-based semiconductor devices has limitations in achieving the required high-speed processing capability. Therefore, much research attention has been focused on next-generation memory devices.²⁾ Among these devices, resistive random access memory (RRAM) has been extensively studied owing to its simple structure, fast operation speed, low power consumption, and excellent scalability

of MIM (metal-insulator-metal).³⁻⁷⁾ The functionality of RRAM relies on the resistive state change of the insulator. The conduction filament is formed through the SET process, where the insulator transitions from a high resistance state (HRS) to a low resistance state (LRS). The filament is ruptured through a RESET operation, which involves a change from LRS to HRS.

Resistance change properties have been observed in binary transition metal oxides such as TiO₂, NiO, and ZnO,⁸⁻¹⁰⁾ as well as in complex oxides like PrCaMnO (PCMO) and Ba_xSr_{1-x}TiO₃.^{11,12)} Among materials with such characteristics, TiO₂ stands out as a binary transition metal oxide due to its

[†]Corresponding author

E-Mail : woo7838@dankook.ac.kr (W.-B. Kim, Dankook Univ.)

*These two authors are equally contributed as first authors.

© Materials Research Society of Korea, All rights reserved.

This is an Open-Access article distributed under the terms of the Creative Commons Attribution Non-Commercial License (<http://creativecommons.org/licenses/by-nc/3.0>) which permits unrestricted non-commercial use, distribution, and reproduction in any medium, provided the original work is properly cited.

high density, simple structure, and fast switching properties.¹³⁾ Therefore, TiO₂ has been widely investigated as a resistive switching (RS) layer in RRAM devices.^{14,15)} The fabrication of TiO₂ thin films can be achieved through vacuum-based or solution-based deposition methods. Vacuum-based methods such as sputter, atomic layer deposition (ALD), and chemical vapor deposition (CVD) have been primarily utilized because of their excellent thickness control and uniform film formation.¹⁶⁾ However, these processes have limitations in terms of cost and complexity.¹⁷⁾ On the other hand, solution-based methods, such as spin coating and hydrothermal methods, offer low-cost, simple processes.^{2,18)} Also, this process has the potential for fabrication of transparent thin films. Among these processes, spin coating has been extensively researched as a method for manufacturing RRAM devices due to its ability to produce thin films and ease of process control.¹⁹⁾ To utilize the advantageous spin coating method, it is necessary to fabricate TiO₂ as a solution-based material. Therefore, in a previous study, we synthesized TiO₂ using the peroxo titanium complex (PTC)-ion method, which is eco-friendly and differs from the conventional TiO₂ fabrication methods.²⁰⁻²²⁾ Moreover, we successfully fabricated a TiN/TiO₂/FTO structure RRAM device using PTC-ion solution and demonstrated successful resistance change properties.²³⁾ The insulator layer of the RRAM device was fabricated using a PTC-ion solution derived from eco-friendly materials, specifically TiO₂. Unlike other solution-based TiO₂ fabrication methods that utilize organo-metal or metal precursors, our PTC-ion synthesis method is safe for human and eco-friendly. However, while a ~45 nm thin film was successfully produced via spin coating, the resulting film's uniformity was inferior to that obtained through vacuum deposition processes. Typically, uniformity and thinness are crucial for achieving low power consumption. Moreover, non-uniform films can lead to the formation of random filaments. Previous research optimized the spin coating process to produce a uniform film, but the issue of random filament formation still persists.

In order to regulate the formation of random filaments in RRAM devices, various studies have been conducted, such as the use of multi-layers or thin metal layers.²⁴⁻²⁷⁾ Nevertheless, the presence of dipoles caused by heterojunctions in multi-layer structures can impede carrier movement, resulting in an increase in the forming voltage.²⁸⁾ Therefore, chan-

ges in device characteristics due to the introduction of precursor materials into TiO₂ thin films have been reported.^{29,30)} Moreover, since the process is solution-based, the precursor material can be introduced into the TiO₂ thin film by simply adding it to the PTC solution. The insertion of metal ions is expected to influence the performance of RRAM devices by affecting filament formation. Various materials, such as Al and Ag, which are used as top electrodes in conductive-bridge random access memory (CBRAM) devices, are potential metal precursors. Among these, Ag can be promising candidate for the insertion of metal precursor. Due to Ag's high mobility characteristics, it is widely used as an upper electrode in RRAM devices and has recently gained attention in the field of neuromorphic computing.^{31,32)} However, as with excessive ion doping, excessive insertion of precursors can lead to deteriorated cycle characteristics, decreased resistance change, and reduced structural stability. Hence, identifying the optimal ratio is crucial.

In general, RRAM devices using TiO₂ as an insulator layer exhibit behavior characteristic of oxygen vacancy resistive access memory (OxRAM), which involves conduction through the formation and rupture of filaments containing oxygen vacancies (V_o).³³⁾ On the other hand, CBRAM relies on a mechanism that involves the formation and rupture of conductive filaments through cations such as Ag or Cu that drift from metal electrodes.³⁴⁾ In the case of an RRAM device fabricated by inserting a metal precursor into the TiO₂ layer, it is expected that a conduction mechanism involving both metallic ions and oxygen vacancies will arise, which is distinct from the general case. Since most insulator layers are fabricated by vacuum deposition, research on directly inserting metal precursors into the insulator layer has not been conducted much yet. Thus, it is crucial to comprehend the fabrication mechanism to effectively apply RRAM devices which inserted metal precursor.

In this study, we aimed to fabricate a TiN/Ag embedded TiO₂/FTO RRAM device through a simple process of embedding Ag nanoparticles in a PTC solution. By optimizing the composition and processing temperature, we successfully confirmed the change in resistance switching characteristics. To investigate the effect of the Ag concentration on resistance change characteristics, we fabricated devices with AgNO₃ concentrations of 0.3, 0.5, and 0.7 at%. We then analyzed the current-voltage (I - V) characteristics of the Ag

embedded RRAMs and identified the appropriate concentration of AgNO_3 precursor. Furthermore, by elucidating the new conduction mechanism, we were able to reduce the operating voltage through the conductive properties of Ag particles. Ultimately, we developed a reliable, eco-friendly, and low-temperature solution process based on PTC-ion.

2. Experimental Procedure

2.1. Device preparation

The PTC-sol was prepared using a jacketed beaker in the same manner as in our previous study while maintaining the reaction temperature below 50°C , titanium hydride (IV) (TiH_2 , 99 %, Sigma-Aldrich) was added to a mixed solution of hydrogen peroxide (H_2O_2 , 30 %, DAEJUNG) and ammonium hydroxide (NH_4OH , 25~30 %, DAEJUNG), after that followed by stirring for 1 h to stabilize the solution.²³⁾ An Ag-PTC-ion solution containing silver nitrate (AgNO_3 , 99 %, Sigma-Aldrich) ions of 0.3 at%, 0.5 at%, and 0.7 at% compared to Ti was prepared. The prepared PTC ion solution at room temperature was heated at 80°C for 10 min and then cooled to a temperature of 15°C or less again. Finally, it was completely dissolved to prepare a transparent Ag-PTC-ion solution. Fluorine doped tin oxide (FTO) glass surface to be used as an electrode was cleaned in order to prepare a uniform TiO_2 thin film. 0.25 mL of the prepared Ag-PTC solution was dripped onto FTO glass through spin coating for 3,000 rpm, 30 s, 3 cycles, and then heat-treated at 100°C to prepare a TiO_2 thin film. Afterward, a titanium nitride (TiN) electrode having a diameter of 0.2 mm and a height of 100 nm was deposited by RF magnetron sputtering through a circular shadow mask.

2.2. Resistive switching test

The I - V curve measurements were conducted in DC

voltage sweep mode using a Keithley 4200A-SCS semiconductor parameter analyzer. For the $\text{TiN}/\text{TiO}_2/\text{FTO}$ devices, DC bias voltages were applied incrementally at 0.05 V/step across a range of 0 ± 8 V. In instances where the FTO bottom electrode was grounded in the TiN/Ag embedded TiO_2/FTO device, the DC bias was applied to the TiN top electrode at a step of 0.05 V within a sweep range of 0 ± 5 V, and a compliance current (C.C) of 0.1 A was implemented. The retention characteristics were verified through retention time measurements, while cycle durability was assessed by analyzing cycle characteristics. Furthermore, the I - V curves were subjected to linear fitting analysis during both positive and negative voltage sweeps to evaluate the device's performance relative to the Ag content.

3. Results and Discussion

3.1. Physical and chemical characteristics

As shown in Fig. 1, it can be confirmed that a TiO_2 thin film is deposited on the pristine FTO glass after 3 cycles of spin coating. As is well known, the thickness and uniformity of the RS layer affect the operating voltage characteristics of the device. So, a thin and uniform film is important for low voltage characteristics. As a result of further enlargement through TEM, it was confirmed that a dense TiO_2 layer was deposited in the range of 50 to 100 nm. In general, PTC-ion solutions have low viscosity and high shrinkage, so it is difficult to prepare a uniform thin film. Through the process used in our previous study, a sufficiently uniform thin film was produced compared to other vacuum deposition processes.²³⁾ To determine the optimal RRAM device, X-ray photoelectron spectroscopy (XPS) analysis was performed to obtain information on the elements and chemical states of the samples. Fig. 2 displays the high-resolution XPS peaks of Ti (2p), O (1s), and Ag (3d) for the (a) pristine TiO_2 , (b) 0.3 at%

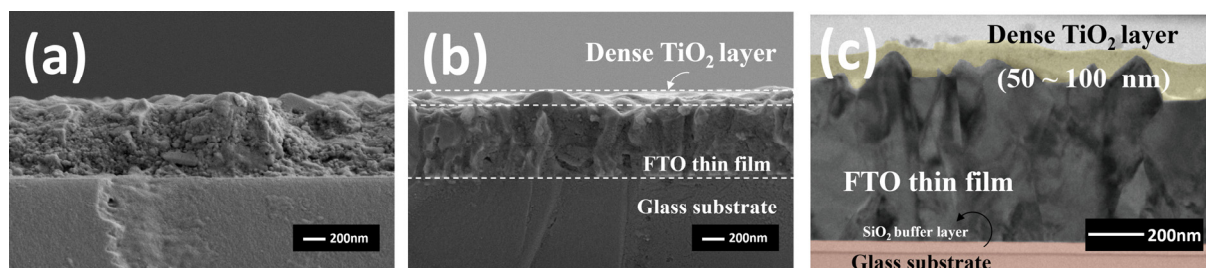


Fig. 1. SEM images of TiO_2 thin films by cycle (a) Pristine-FTO (b) 3 cycles TiO_2 coated FTO, TEM images (c) of 3 cycles TiO_2 coated FTO.

embedded TiO₂ and (c) 0.5 at% embedded TiO₂ RRAM devices. The Ti (2p_{3/2}) peaks were respectively 458.17 eV and 456.86 eV in (a). Also, 0.3 at% Ag embedded TiO₂ RRAM device in (b) show characteristic peaks at 458.18 eV and 456.83 eV, which correspond to Ti⁴⁺ and Ti³⁺, respectively.²³⁾ Similarly, according to (c), the 0.5 at% Ag embedded TiO₂ RRAM device appear at 458.18 eV and 456.98 eV. It was confirmed that TiO₂ was successfully formed in all samples. Compared to the (a), intensity of Ti was decreased by the addition of Ag. It goes with the formation of Ti³⁺ also decreased. Ti³⁺ is generated by the formation of oxygen vacancies, and it acts as a defect.³⁵⁾ However, it shows that the ratio of Ti³⁺ in (c) is increased compared to (b). This seems to affect oxygen vacancies by increasing the formation of Ag-O bonds due to excessive Ag intercalation. The

presence of many oxygen vacancies can lead to a decrease in operating voltage. However, as SET/RESET switching is repeated, cycle stability may be adversely affected due to the reduction of oxygen ions. Additionally, the defect site inside can act as an electron trap site and can have an electrical effect on the device. The O (1s) peak exhibits characteristic peaks at 529.67 eV, 531.33 eV, which correspond to Ti-O, -OH respectively. In (b), the binding energy of O (1s) are 529.64 eV, 530.73 eV, 532.07 eV, and 532.4 eV, which correspond to Ti-O, Ag-O, -OH, and O₂.^{36,37)} Similarly, respectively bondings were characterized at 529.7 eV, 530.79 eV, 532.13 eV, and 532.52 eV in (c). In (b) and (c), the presence of Ag-O peaks was confirmed following the insertion of Ag. A notable change was observed in the -OH peak. Unlike the RRAM devices in the (a), both samples showed a

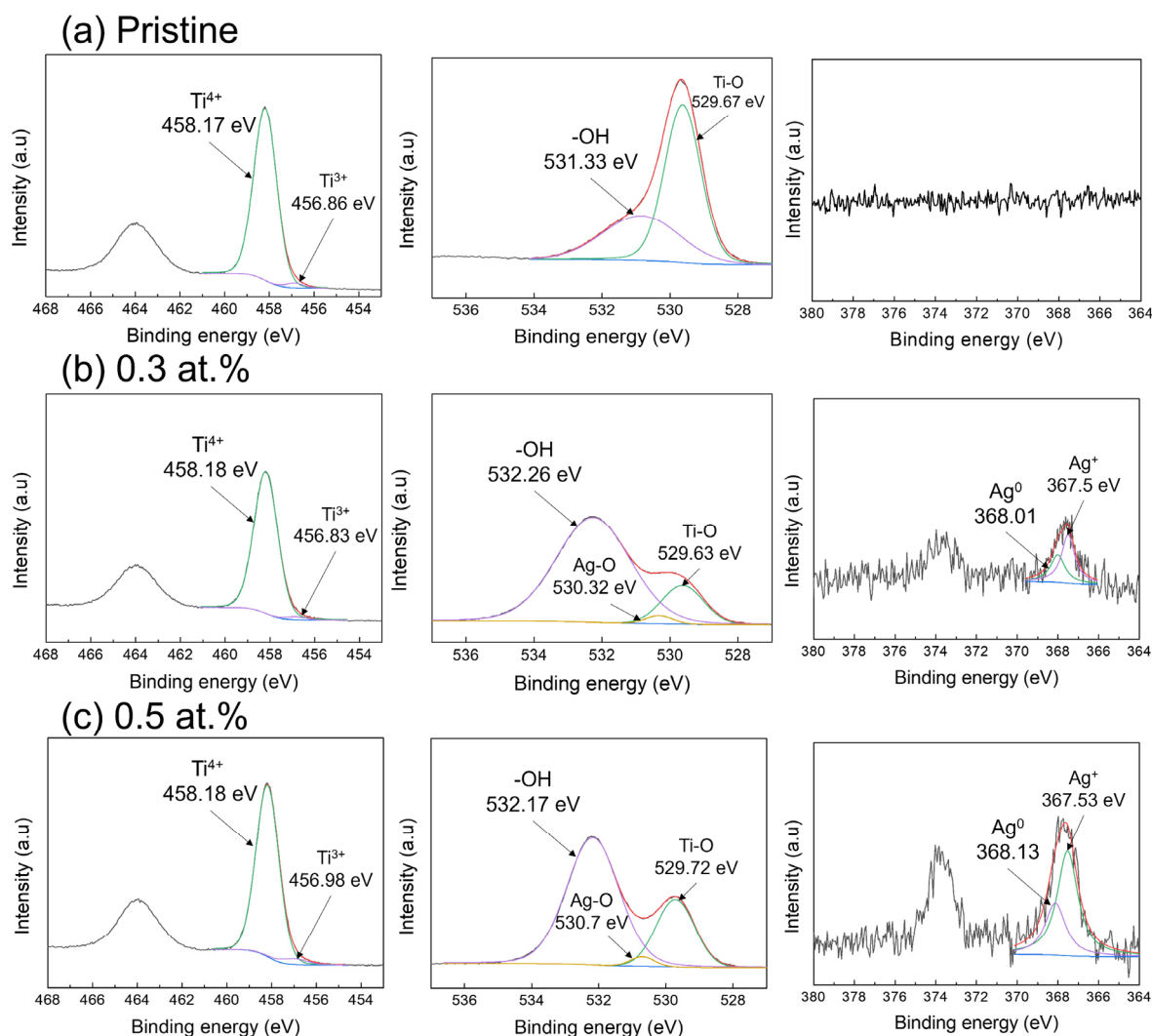


Fig. 2. Ti (2p), O (1s), Ag (3d) XPS spectra of TiO₂ thin film (a) Pristine TiO₂ RRAM, (b) 0.3 at% embedded RRAM device, (c) 0.5 at% Ag embedded RRAM device.

significant increase in the area of the -OH peak, which seems to have resulted from the interaction between Ag and TiO₂. The amount of Ag-O bonding slightly increased with the addition of Ag. Unlike (a), Ag (3d_{5/2}) spectra of (b) and (c) were characterized at 367.67 eV and 367.62 eV, respectively. Each sample is divided into 367.5 eV, 368.01 eV, and 367.53 eV, 368.13 eV, which correspond to Ag⁺ and Ag⁰, respectively.³⁸⁾ An increase in intensity was confirmed with the addition of Ag. Additionally, Ag exists more as Ag⁺ than Ag⁰, which corresponds to the Ag-O peak in the O (1s) peak. The binding energy of bulk Ag (3d_{5/2}) was assigned at 368.3 eV, and both samples were shifted to the lower position.³⁹⁾ These results are likely due to the strong interaction of electrons moving from TiO₂ to metallic Ag.³⁷⁾

3.2. Resistive switching characteristics

Based on the results of previous studies, the basic characteristics of the Ag embedded TiO₂ RRAM devices were investigated by applying a voltage sweep range of 0 ± 8 V with a consistent C.C value of 0.1 A.²³⁾ Fig. 3 illustrates the *I-V* curve under the condition of 0.3 at% Ag embedded TiO₂ RRAM. Initially, during the positive voltage sweep, the current level gradually increased, leading to a SET operation at +3.7 V. This was followed by maintaining the LRS during the reverse voltage sweep, where the RESET operation occurred at -3.7 V. The investigated *I-V* curve results showed a variance from those of conventional OxRRAM. Firstly, compared to OxRRAM, the initial resistance value was increased by four orders of magnitude, resulting in a low initial resistance value of 10⁻⁶. Furthermore, it was observed that the SET/RESET voltage significantly decreased to -3.7 V/3.7 V according to the voltage sweep range. This indicates that the addition of Ag altered the resistance characteristics of the TiO₂ layer, and the material forming filaments shifted

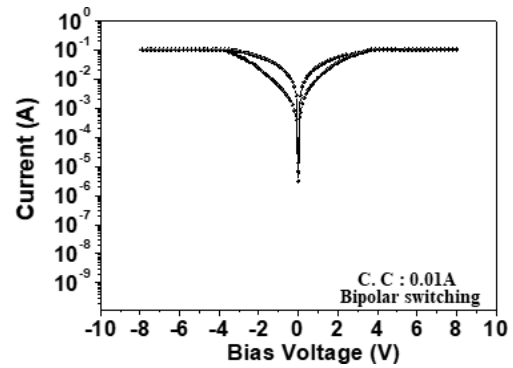


Fig. 3. 0 ± 8 V voltage sweep range, 0.3 at% Ag embedded TiO₂ RRAM *I-V* characteristics under 0.1A C.C condition.

to metallic filaments, exhibiting characteristics of CBRAM. As the SET/RESET voltage range decreased, sweeping at unnecessarily high voltage ranges could stress the device. Therefore, the voltage sweep range was reduced to ±5 V, and simultaneously, the C.C was decreased by one order of magnitude to apply a current of 10 mA. Under these modified conditions, Fig. 3 characterizes the *I-V* curves of Ag embedded TiO₂ RRAM with varying Ag content.

Electrical analysis was conducted on TiN/Ag-embedded TiO₂/FTO RRAM devices with varying Ag content (0.3 at%, 0.5 at%, and 0.7 at%), to investigate the effect of Ag concentration on resistance switching characteristics. Fig. 4(a) illustrates the *I-V* curve of the RRAM device with 0.3 at% Ag, indicating typical nonvolatile bipolar RS behavior. During the negative voltage sweep, the current gradually increases, and a SET process (transition from HRS to LRS) occurs due to a rapid rise in current level at V_{set} : ~-3 V. On the other hand, during the positive voltage sweep, LRS is maintained, and a RESET process (transition from LRS to HRS) occurs through a sudden drop in current at V_{reset} : ~3 V. The TiN/0.3 at% Ag-embedded TiO₂/FTO RRAM device showed successful RS characteristics, reaching the initial resistance value

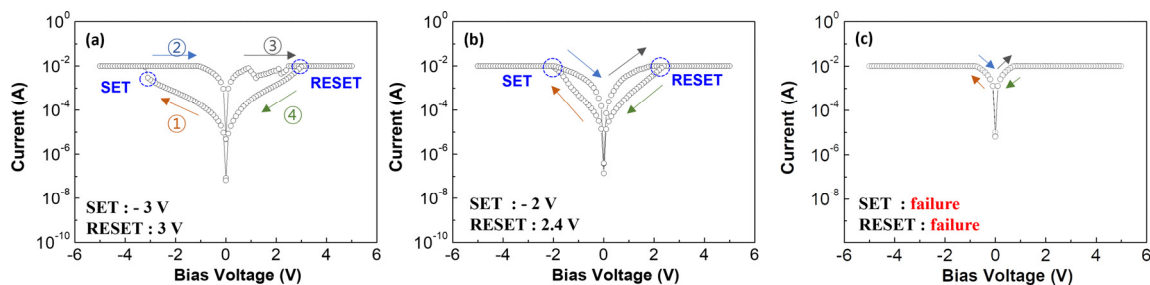


Fig. 4. Switching behavior (SET, RESET) of TiN/Ag-embedded TiO₂/FTO RRAM device according to compliance current and voltage sweep range (a) 0.3 at%, (b) 0.5 at%, (c) 0.7 at%.

of 10-8. Similarly, the RRAM device embedded with 0.5 at% Ag also showed RS behavior, as shown in Fig. 4(b), with a gradual rise in current during the negative voltage sweep, and a SET process at V_{set} : ~ -2 V. During the positive voltage sweep, LRS is maintained, and a RESET process occurs at V_{reset} : ~ 2.4 V. Therefore, the TiN/0.5 at% Ag-embedded TiO₂/FTO RRAM device also showed successful RS characteristics, reaching an initial resistance value of 10^{-8} . However, when the Ag content was 0.7 at%, complete ohmic conduction characteristics were observed, with the absence of SET and RESET processes. The initial resistance of the TiN/0.7 at% Ag embedded TiO₂/FTO RRAM device was greatly reduced, with an initial resistance value of 10^{-6} , unlike the 0.3 at% and 0.5 at% embedded RRAM devices. Hence, at high Ag concentrations, it appears that the resistance change layer does not function as an insulator. While the RRAM devices with 0.3 at% and 0.5 at% Ag were successfully behaved as RRAM devices, the 0.7 at% embedded RRAM device did not. As the content of Ag increased from 0.3 at% to 0.5 at%, the V_{set} and V_{reset} of the RRAM device decreased, likely due to an increase in the proportion of Ag ions forming filaments. Furthermore, the V_{set} and V_{reset} of the RRAM device with 0.3 at% and 0.5 at% embedded Ag were significantly reduced compared to the TiN/TiO₂/FTO RRAM device fabricated in a previous study, with a reduction of about 4 V or more each.²³⁾ Despite having the same thickness, the values of V_{set} and V_{reset} decreased by more than half depending on the Ag content. In general, the resistance change characteristic in binary oxide-based devices is caused by the formation and rupture of filaments by oxygen ions.⁴⁰⁾ However, in the case of TiO₂ layers containing Ag, a change in the conduction mechanism is expected to occur due to the formation of a conduction bridge by the movement of Ag ions.

Fig. 5 illustrates the cycle characteristics of the RRAM device according to content of Ag. As Ag is inserted, cycle performance is improved. In Fig. 5(a), resistance change characteristics no longer appear after 4 cycles. This is because O²⁻ ions generated by cycle repetition in the RS layer made of pristine TiO₂ combine with each other and lose as O². However, in the case of Fig. 5(b), the number of escaped O²⁻ is reduced due to the presence of Ag, resulting in improved stability. And it shows that the resistance change characteristics were consistently maintained up to 10 cycles. The insertion of Ag ostensibly enhances cycle performance. On the other hand, the RRAM device containing 0.5 at% Ag embedded TiO₂ in Fig. 5(c) could not maintain the resistance change characteristics as the cycle number increased, and the device showed ohmic conduction behavior after only 5 cycles. While low Ag content improves device stability by reducing the loss of O²⁻ ions, leading to enhanced cycle performance, a higher Ag content (0.5 at%) introduces challenges. The RRAM device with 0.5 at% Ag exhibits ohmic conduction behavior after a limited number of cycles due to the incomplete oxidation of Ag filaments. Similar to the behavior of a typical CBRAM device, when an opposite voltage is applied to the device, the Ag filament is oxidized to Ag⁺.⁴¹⁾ The excessive Ag leads to a build-up of unoxidized Ag atoms, adversely affecting the device's resistive switching characteristics.⁴²⁾ Therefore, the application of the RRAM device containing 0.5 at% Ag as a reliable memory device is limited. In addition to cycle performance, the retention time is an essential factor in evaluating the performance of a memory device.⁴³⁾

The retention characteristics of the pristine TiO₂ and 0.3 at% Ag-embedded TiO₂ RRAM device are presented in Fig. 6. Both devices were shown a stable current level in both HRS and LRS for a period of 3,600 s, which is consistent

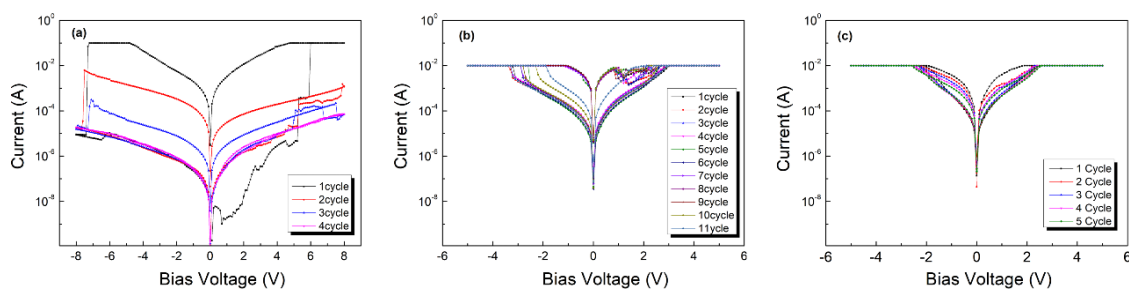


Fig. 5. Cycle characteristics under (a) Pristine TiO₂ RRAM, (b) 0.3 at% Ag embedded TiO₂ RRAM and (c) 0.5 at% Ag embedded TiO₂ RRAM.

with the retention behavior observed in typical RRAM devices.⁴²⁾ Additionally, the ON/OFF ratio for the pristine device (a) was measured at 10^4 , and for (b), it was found to be greater than 10^3 , aligning with the values derived from the I - V curve. For a non-volatile memory to be useful in practical applications, the ON/OFF ratio value should typically be at least 10 times higher than the reported value.⁴⁴⁻⁴⁶⁾ Therefore, the observed ON/OFF ratio value of 3 orders of magnitude or greater confirms the suitability of the implemented device for use as a non-volatile memory. In addition, considering the above cycle stability, it was confirmed that Ag was inserted at 0.3 at% as optimal.

3.3. Resistive switching mechanism

Previous measurements of the current-voltage characteristics have indicated that the TiN/Ag embedded TiO₂/FTO device operates through filament formation and migration of Ag ions as well as filament formation by oxygen vacancy. However, to fully comprehend the dominant mechanism of the TiN/Ag-embedded TiO₂/FTO device for its practical application, it is necessary to confirm the conduction mechanism. Therefore, we analyzed the conduction mechanism of 0.3 and 0.5 at% Ag samples, where resistance change characteristics were observed. Fig. 6 show the I - V curve and double- logarithmic plot of TiN/Ag-embedded TiO₂/FTO devices with 0.3 at% and 0.5 at% Ag content. The conduction mechanism was confirmed by performing linear fitting of I - V curves during positive and negative voltage sweeps. As shown in Fig. 7(a), for the 0.3 at% Ag sample, the slope at high voltage during the negative bias sweep was found to be 2 or more, and a sudden increase in current was observed, confirming the dominance of the SCLC mechanism. The

linear fitting of the 0.3 at% Ag sample also showed a slope of 1.4 during the negative bias sweep at high voltage. Typically, a slope close to 1 indicates either no current flow due to high resistance or ohmic conduction resulting from internal thermal carriers. However, since the slope was found to be higher than 1, the conduction mechanism can be attributed to Schottky emission ($\log(I) \propto V^{0.5}$) during the low voltage range of 0~1 V in the HRS state. The direction and shape of filament formation by Ag ions are determined by the mobility of cations and the reduction rate of ions in the dielectric.³⁷⁾ In the case of the TiN/Ag embedded TiO₂/FTO device, Ag ions move to the TiN electrode at a negative bias to form a tip, as the mobility of Ag ions is higher than the reduction rate. Therefore, the gap between the upper and lower electrodes is reduced due to the formed tip, resulting in a reduction in resistance and facilitating filament formation, leading to conduction by Schottky emission.

Subsequently, at voltages between 2 to 3.1 V, the 0.3 at% Ag sample exhibits a slope of 3.1, accompanied by a sharp increase in current, which is dominated by the trap-limited space charge limited current (SCLC) conduction mechanism ($I \propto V^2$). At this point, the injected carriers conduct a more significant role in determining the conduction characteristics due to an increase in carrier injection as compared to thermally generated carriers in the thin film. This phenomenon arises from the formation of a conductive path through the filament, which has been previously reported in Ti/Al₂O₃/AgNPs/Al₂O₃/p-Si structures, where Ag atoms and oxygen vacancies form filaments together.⁴¹⁾ The conductivity is substantially enhanced during this period, leading to the SET process. Oxygen vacancies (V_o^+) migrate towards TiN in response to the negative voltage applied to the top electrode,

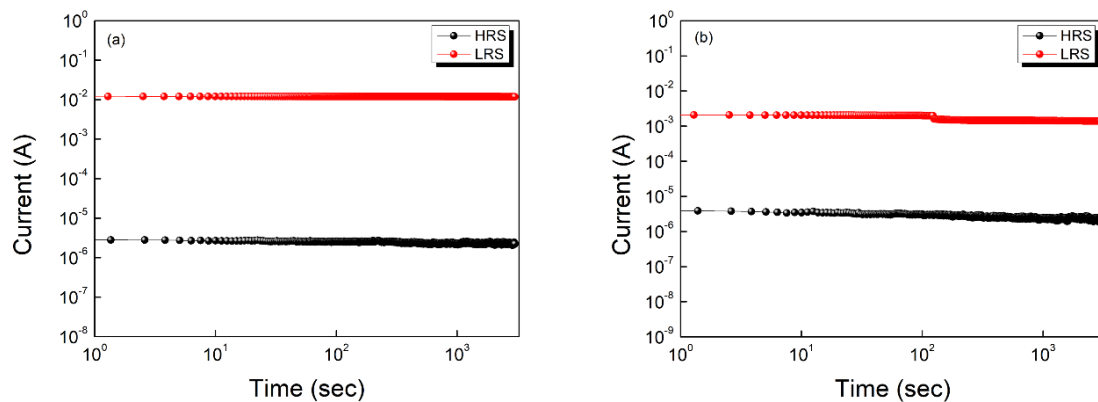


Fig. 6. Retention time characteristics under (a) Pristine TiO₂ RRAM, (b) 0.3 at% Ag embedded TiO₂ RRAM.

forming filaments that follow the previously formed Ag ion tips. Additionally, Ag particles act as seeds in the conductive filament, reducing the randomness of filament formation and decreasing the conductivity path of the filament.⁴⁷⁾ In the following -1 V to 0 V sweep range, the slope of the 0.3 at% Ag sample is 1.2, indicating ohmic contact ($I \propto V$) conduction. Similarly, during the 0 V to 0.9 V sweep range, which corresponds to a positive bias, the slope is 0.96, confirming the ohmic contact ($I \propto V$) characteristic.⁴⁸⁾ This indicates that the positive bias applied to the top electrode is insufficient to break the hybrid filament composed of Ag atoms and oxygen vacancies. After that, the RESET voltage is reached, and the slope up to ~2 V is 4.9, demonstrating the trap-limited SCLC conduction mechanism. The slope during the 2 V to 0 V range is 1.7, following the Schottky emission mechanism. In the case of the 0.5 at% Ag sample, the result of the linear fitting in Fig.7(b) shows that the slope at high voltage has a value of 2 or more during the sweep to negative bias, accompanied by a sudden increase in current, confirming the dominance of the SCLC mechanism. However, the linear fitting result of the RRAM device containing 0.5 at% Ag, as shown in Fig.7(b), exhibits a high slope. As the Ag content

increases, the amount of Ag that forms the filament increases, exhibiting characteristics that are consistent with the ionic conduction model. This outcome indicates that, unlike the 0.3 at% embedded RRAM, Ag becomes the primary component constituting the filament. The slope of the ionic conduction model can be calculated as follows.⁴⁹⁾

$$\text{Ln } J \propto \text{Ln } V - \left(\text{Ln } T + \frac{d}{T} \right) \quad (1)$$

The current density J , applied voltage V , temperature T , and a constant d are the parameters involved in the calculation of the slope in Fig. 7(b). Specifically, the HRS in Fig. 7(b) exhibited a slope of 1.6, while the slope increased to 4.1 in the LRS after the SET voltage was applied. The LRS slope was maintained at 1.7. When the RESET voltage was applied, a high slope of 4.8 was observed, although no current jumping was detected. This behavior is typical of CBRAM, where the metallic ion forming the filament is reduced to the top electrode during RESET operation and disappears within the insulator. However, even after reduction, Ag ions remain inside the insulator in Ag-inserted devices. As demonstrated

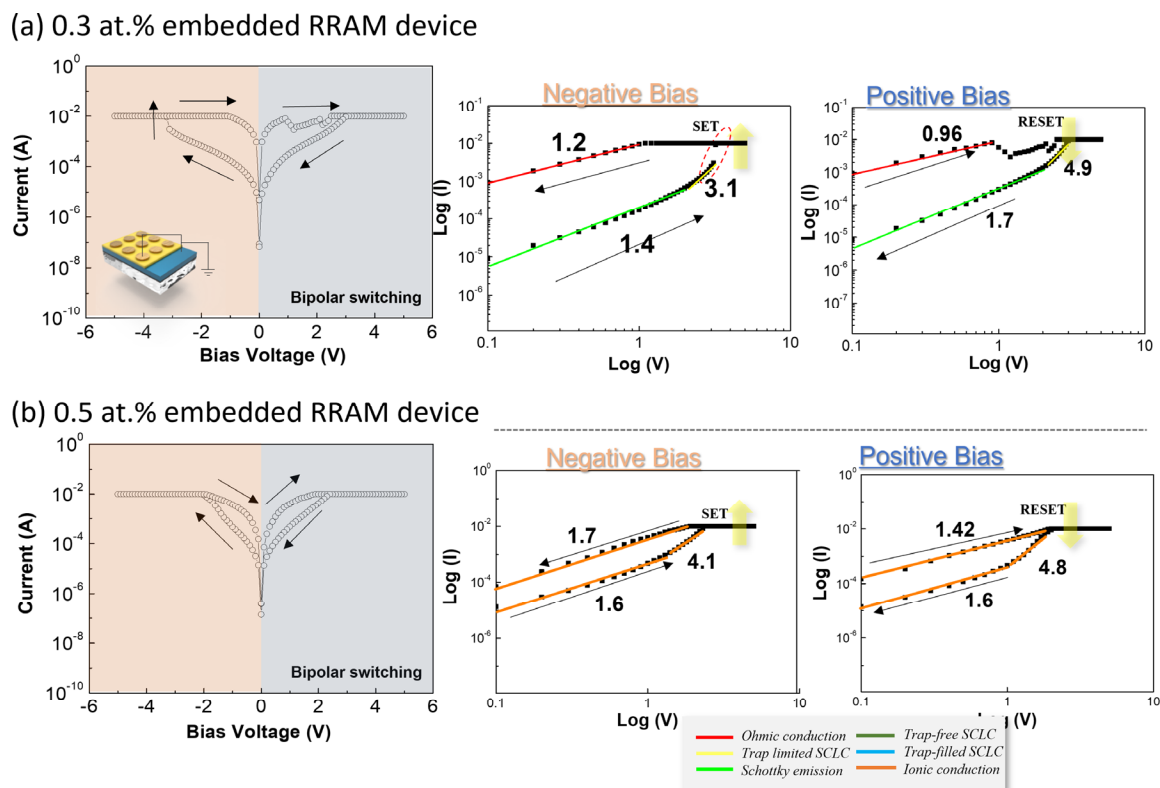


Fig. 7. I - V curve of Ag embedded TiO₂ RRAM (a) 0.3 at% Ag embedded RRAM and (b) 0.5 at% Ag embedded RRAM.

by the previous cycle characteristics, excessive Ag content inside the insulator reduces device resistance and degrades RRAM performance, such as the ON/OFF ratio. Therefore, these results indicate that the electrical behavior and conduction mechanism in the RRAM device are affected by the Ag content, and the optimal performance is achieved when 0.3 at% of Ag is incorporated.

Based on the results described above, we present a model of filament formation through the movement of Ag ions and oxygen vacancies, as illustrated in Fig. 8. In the pristine state, before any voltage is applied, Ag is present in the TiO_2 layer in the form of Ag^+ and Ag atoms.²⁸⁾ TiO_2 generally exists in a non-stoichiometric form, TiO_{2-x} , where x represents a non-stoichiometric amount.^{50,51)} The presence of non-stoichiometric amounts is typically caused by gaps in titanium or oxygen vacancies, with the latter resulting from insufficient oxygen supply during the deposition of TiO_2 .⁵²⁾ As such, oxygen vacancies are already present in the TiO_2 layer even before the application of any voltage. When a negative voltage is applied, Ag ions in the TiO_2 layer move towards the TiN electrode, while Ag atoms are oxidized and also move towards the TiN electrode in the form of Ag^+ . The moved Ag ions are reduced to form Ag atoms, which then form tips.^{53,54)} Meanwhile, O^{2-} ions move towards the positively biased lower electrode, where they are converted into O_2 molecules. As a result, numerous oxygen vacancies are formed at the lower electrode interface.⁵⁵⁾ As the negative bias becomes stronger, the formation of oxygen vacancies increases from the FTO direction (positive bias), leading to the formation of filaments. At the same time, Ag filaments are formed from the TiN direction, which is the opposite direction. The two filaments eventually connect, leading to the SET process. When a positive bias is applied to the upper electrode, the joule heat generated by the thermal effect causes the oxygen

vacancy and Ag atom filaments to be cut, leading to the RESET process. However, due to the lower activation energy of oxygen vacancies, the breakdown of the filament occurs faster than that of Ag atom filaments.⁴⁷⁾ Additionally, most of the positive bias applied to the upper part of the two positive charge types, oxygen vacancies, is pushed to the opposite side, resulting in the rupture of the filament. In contrast, in the case of Ag atom filaments, an electrochemical process involving overvoltage is required for Ag, which is an atom, to return to ions. As a result, the rupture of the filament mainly occurs in oxygen vacancy filaments, while Ag filaments remain almost unchanged.

4. Conclusion

In this study, we confirmed the electrical properties of TiN/Ag-embedded TiO_2/FTO RRAM devices fabricated using an eco-friendly PTC-ion solution-based process with AgNO_3 precursor added in varying concentrations. Comparing the I - V curves of devices with varying AgNO_3 precursor concentrations reveals that RRAM devices with 0.3 at% and 0.5 at% Ag content display resistive switching (RS) characteristics, whereas devices with 0.7 at% Ag do not. The device with 0.5 at% Ag shows lower switching voltages than the one with 0.3 at% but has a reduced difference in current levels between high and low resistance states and lower initial resistance. Additionally, the 0.3 at% Ag device retains its switching characteristics for over 10 cycles, outperforming the 0.5 at% Ag device, which fails after 5 cycles.

Therefore, it was confirmed that the addition of Ag to the TiN/ TiO_2 /FTO RRAM device can effectively prevent random filament formation and produce uniform RRAM devices with desirable electrical characteristics. By analyzing the I - V curves of different Ag content samples, it was found that 0.5

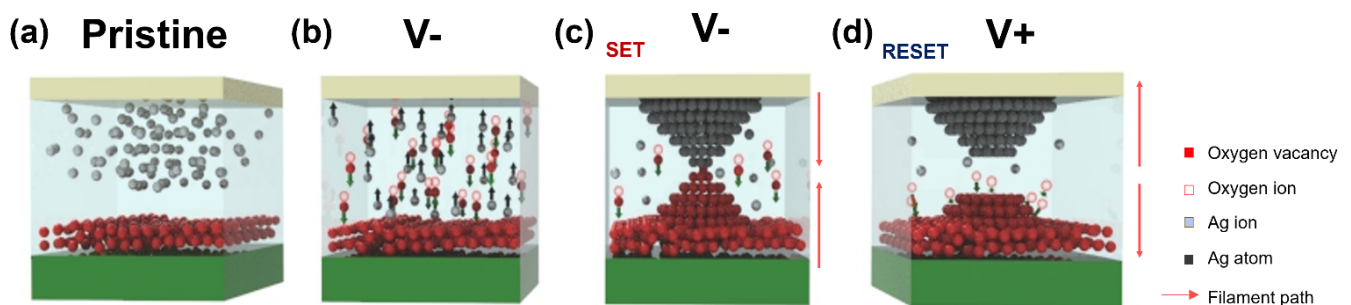


Fig. 8. A model of resistive switching mechanism in TiN/Ag embedded TiO_2/FTO memory device.

at% Ag content provided only suitable I - V characteristics, while 0.3 at% Ag content showed suitable I - V curve, ON/OFF ratio and long retention times. The conduction mechanism of the each RRAM device was also analyzed, showing that the electrical behavior and conduction mechanism varied with the Ag content. Through optimization of the Ag content, this study successfully overcame the limitations of the TiN/TiO₂/FTO RRAM device, reducing SET/RESET voltage and C.C current, and improving cycle characteristics. In conclusion, our research presents a thorough analysis of cycle performance and retention characteristics under varying Ag contents, providing a comprehensive understanding of the necessary trade-offs and optimization strategies for developing high-density, low-power RRAM applications. This paves the way for its application in the advanced fabrication processes of RRAM devices, signifying a substantial step forward in the field.

Acknowledgement

This work was supported by the National Research Foundation of Korea (NRF) grant funded by the Korea government (MIST) (No. 2022R1A2C1006148) and This research was supported by Nano · Material Technology Development Program through the National Research Foundation of Korea (NRF) funded by the Ministry of Science, ICT and Future Planning (2009-0082580).

Declaration of Competing Interest

The authors declare that they have no known competing financial interests or personal relationships that could have appeared to influence the work reported in this paper.

References

1. S. Gao, X. Yi, J. Shang, G. Liu and R.-W. Li, Chem. Soc. Rev., **48**, 1531 (2019).
2. J. Bera, A. Betal, A. Sharma, U. Shankar, A. K. Rath and S. Sahu, ACS Appl. Nano Mater., **5**, 8502 (2022).
3. J. S. Meena, S. M. Sze, U. Chand and T.-Y. Tseng, Nanoscale Res. Lett., **9**, 526 (2014).
4. H. Lee, P. Chen, T. Wu, Y. Chen, C. Wang, P. Tzeng, C. Lin, F. Chen, C. Lien and M.-J. Tsai, in Proceedings of the 2008 IEEE International Electron Devices Meeting (San Francisco, CA, December 2008) p. 1-4.
5. Y. Hosoi, Y. Tamai, T. Ohnishi, K. Ishihara, T. Shibuya, Y. Inoue, S. Yamazaki, T. Nakano, S. Ohnishi and N. Awaya, in Proceedings of the 2006 International Electron Devices Meeting (San Francisco, CA, December 2006) p. 1-4.
6. R. Waser and M. Aono, Nat. Mater., **6**, 833 (2007).
7. D. Kumar, R. Aluguri, U. Chand and T.-Y. Tseng, Ceram. Int., **43**, S547 (2017).
8. M. J. Lee, S. I. Kim, C. B. Lee, H. Yin, S. E. Ahn, B. S. Kang, K. H. Kim, J. C. Park, C. J. Kim and I. Song, Adv. Funct. Mater., **19**, 1587 (2009).
9. B. Choi, D. S. Jeong, S. Kim, C. Rohde, S. Choi, J. Oh, H. Kim, C. Hwang, K. Szot and R. Waser, J. Appl. Phys., **98**, 033715 (2005).
10. F. M. Simanjuntak, D. Panda, K.-H. Wei and T.-Y. Tseng, Nanoscale Res. Lett., **11**, 368 (2016).
11. A. Sawa, Mater. Today, **11**, 28 (2008).
12. F. Pontes, E. Longo, E. Leite and J. A. Varela, Thin Solid Films, **386**, 91 (2001).
13. M.-J. Lee, C. B. Lee, D. Lee, S. R. Lee, M. Chang, J. H. Hur, Y.-B. Kim, C.-J. Kim, D. H. Seo and S. Seo, Nat. Mater., **10**, 625 (2011).
14. L. Qingjiang, A. Khiat, I. Salaoru, C. Papavassiliou, X. Hui and T. Prodromakis, Sci. Rep., **4**, 4522 (2014).
15. M. H. Lee, K. M. Kim, G. H. Kim, J. Y. Seok, S. J. Song, J. H. Yoon and C. S. Hwang, Appl. Phys. Lett., **96**, 152909 (2010).
16. S. M. George, Chem. Rev., **110**, 111 (2010).
17. C. Liu, L.-G. Wang, K. Qin, Y.-Q. Cao, X.-J. Zhang, D. Wu and A.-D. Li, IEEE Trans. Electron Devices, **65**, 4674 (2018).
18. M. Xiao, K. P. Musselman, W. W. Duley and Y. N. Zhou, ACS Appl. Mater. Interfaces, **9**, 4808 (2017).
19. P. S. Schulze, K. Wienands, A. J. Bett, S. Rafizadeh, L. E. Mundt, L. Cojocar, M. Hermle, S. W. Glunz, H. Hillebrecht and J. C. Goldschmidt, Thin Solid Films, **704**, 137970 (2020).
20. H. Park, S. Joo, J.-P. Choi and W.-B. Kim, J. Powder Mater., **22**, 396 (2015).
21. S. H. Ji, H. Park, D. Kim, D. H. Han, H. W. Yun and W.-B. Kim, Korean J. Mater. Res., **29**, 183 (2019).
22. J. Lee, J. Hwang, H. Park, T. Sekino and W.-B. Kim, Appl. Surf. Sci., **540**, 148399 (2021).
23. J. Lee, R. N. Kim, K.-R. Park and W.-B. Kim, Appl. Surf. Sci., **562**, 150170 (2021).
24. C.-C. Hsieh, A. Roy, A. Rai, Y.-F. Chang and S. K. Banerjee, Appl. Phys. Lett., **106**, 173108 (2015).
25. S. Kim, T.-H. Kim, H. Kim and B.-G. Park, Appl. Phys.

- Lett., **117**, 202106 (2020).
26. D. Panda, C. Chu, A. Pradhan, S. Chandrasekharan, B. Pattanayak, S. Sze and T. Tseng, *Semicond. Sci. Technol.*, **36**, 045002 (2021).
 27. Y.-J. Choi, M.-H. Kim, S. Bang, T.-H. Kim, D. K. Lee, K. Hong, C. S. Kim, S. Kim, S. Cho and B.-G. Park, *IEEE Access*, **8**, 228720 (2020).
 28. Y.-P. Hsiao, W.-L. Yang, L.-M. Lin, F.-T. Chin, Y.-H. Lin, K.-L. Yang and C.-C. Wu, *Microelectron. Reliab.*, **55**, 2188 (2015).
 29. N. Naseri, H. Kim, W. Choi and A. Moshfegh, *Int. J. Hydrogen Energy*, **37**, 3056 (2012).
 30. E. Albitter, M. Valenzuela, S. Alfaro, G. Valverde-Aguilar and F. Martínez-Pallares, *J. Saudi Chem. Soc.*, **19**, 563 (2015).
 31. Z. Wang, S. Joshi, S. E. Savel'ev, H. Jiang, R. Midya, P. Lin, M. Hu, N. Ge, J. P. Strachan and Z. Li, *Nat. Mater.*, **16**, 101 (2017).
 32. H. Yeon, P. Lin, C. Choi, S. H. Tan, Y. Park, D. Lee, J. Lee, F. Xu, B. Gao and H. Wu, *Nat. Nanotechnol.*, **15**, 574 (2020).
 33. H.-S. P. Wong, H.-Y. Lee, S. Yu, Y.-S. Chen, Y. Wu, P.-S. Chen, B. Lee, F. T. Chen and M.-J. Tsai, *Proc. IEEE*, **100**, 1951 (2012).
 34. K.-C. Kwon, M.-J. Song, K.-H. Kwon, H.-V. Jeoung, D.-W. Kim, G.-S. Lee, J.-P. Hong and J.-G. Park, *J. Mater. Chem. C*, **3**, 9540 (2015).
 35. R.-C. Fang, Q.-Q. Sun, P. Zhou, W. Yang, P.-F. Wang and D. W. Zhang, *Nanoscale Res. Lett.*, **8**, 92 (2013).
 36. T. Wang, H. Xiao, Y. Gao, J. Xu, Z. Zhang, H. Bian and T. Sun, *J. Mater. Sci.: Mater. Electron.*, **31**, 11496 (2020).
 37. C. Su, L. Liu, M. Zhang, Y. Zhang and C. Shao, *CrystEng Comm*, **14**, 3989 (2012).
 38. M. Padilla Villavicencio, A. Escobedo Morales, M. d. L. Ruiz Peralta, M. Sánchez-Cantú, L. Rojas Blanco, E. Chigo Anota, J. H. Camacho García and F. Tzompantzi, *Catal. Lett.*, **150**, 2385 (2020).
 39. H. W. Chen, Y. Ku and Y. L. Kuo, *Chem. Eng. Technol.*, **30**, 1242 (2007).
 40. A. Regoutz, I. Gupta, A. Serb, A. Khiat, F. Borgatti, T. L. Lee, C. Schlueter, P. Torelli, B. Gobaut and M. Light, *Adv. Funct. Mater.*, **26**, 507 (2016).
 41. S. Yu and H.-S. P. Wong, *IEEE Trans. Electron Devices*, **58**, 1352 (2011).
 42. L. Gao, Y. Li, Q. Li, Z. Song and F. Ma, *Nanotechnology*, **28**, 215201 (2017).
 43. Y. Chen, H. Lee, P. Chen, P. Gu, C. Chen, W. Lin, W. Liu, Y. Hsu, S. Sheu and P. Chiang, in *Proceedings of the 2009 IEEE International Electron Devices Meeting (IEDM)* (Baltimore, MD, December 2009) p. 1-4.
 44. W. Guan, S. Long, R. Jia and M. Liu, *Appl. Phys. Lett.*, **91**, 062111 (2007).
 45. A. Hao, M. Ismail, S. He, N. Qin, W. Huang, J. Wu and D. Bao, *RSC Adv.*, **7**, 46665 (2017).
 46. Y. Huang, Z. Shen, Y. Wu, X. Wang, S. Zhang, X. Shi and H. Zeng, *RSC Adv.*, **6**, 17867 (2016).
 47. Y.-L. Chung, W.-H. Cheng, J.-S. Jeng, W.-C. Chen, S.-A. Jhan and J.-S. Chen, *J. Appl. Phys.*, **116**, 164502 (2014).
 48. Y. Xia, B. Sun, H. Wang, G. Zhou, X. Kan, Y. Zhang and Y. Zhao, *Appl. Surf. Sci.*, **426**, 812 (2017).
 49. J. Jiang, D. G. Lim, K. Ramadoss and S. Ramanathan, *Solid-State Electron.*, **146**, 13 (2018).
 50. D.-H. Kwon, K. M. Kim, J. H. Jang, J. M. Jeon, M. H. Lee, G. H. Kim, X.-S. Li, G.-S. Park, B. Lee and S. Han, *Nat. Nanotechnol.*, **5**, 148 (2010).
 51. U. Diebold, *Surf. Sci. Rep.*, **48**, 53 (2003).
 52. A. Janotti, J. Varley, P. Rinke, N. Umezawa, G. Kresse and C. Van de Walle, *Phys. Rev. B*, **81**, 085212 (2010).
 53. J. J. Yang, F. Miao, M. D. Pickett, D. A. Ohlberg, D. R. Stewart, C. N. Lau and R. S. Williams, *Nanotechnology*, **20**, 215201 (2009).
 54. T. Tsuruoka, K. Terabe, T. Hasegawa and M. Aono, *Nanotechnology*, **21**, 425205 (2010).
 55. J. J. Yang, J. Borghetti, D. Murphy, D. R. Stewart and R. S. Williams, *Adv. Mater.*, **21**, 3754 (2009).

Author Information

Won Jin Kim

Student, Department of Foundry Engineering, Dankook University

Jinho Lee

Student, Department of Energy Engineering, Dankook University

Ryun Na Kim

Student, Department of Energy Engineering, Dankook University

Donghee Lee

Student, Department of Energy Engineering, Dankook University

Woo-Byoung Kim

Professor, Department of Foundry Engineering, Dankook University

Professor, Department of Energy Engineering, Dankook University